UDK 620.177.6:621.56:532.57:621.771
Original scientific article/Izvirni znanstveni članek

ISSN 1580-2949
MTAEC9, 55(3)377(2021)

METHOD ACHIEVING COOLING UNIFORMITY AND OPTIMAL PLATE-CURVATURE DURING ULTRA-FAST COOLING IN A HSM

ENAKOMERNO OHLAJANJE IN METODA DOSEGANJA OPTIMALNE UKRIVLJENOSTI TRAKU MED ULTRA HITRIM OHLAJANJEM V VALJARNI VROČIH TRAKOV

Lian-yun Jiang[1*], Yao-yu Wei[1], Zhen-lei Li[2], Li-feng Ma[1]

[1]School of Mechanical Engineering, Taiyuan University of Science and Technology, Taiyuan 030024, PR China
[2]State Key Laboratory of Rolling and Automation, Northeastern University, Shenyang 110819, PR China

Prejem rokopisa – received: 2021-01-30; sprejem za objavo – accepted for publication: 2021-02-22

doi:10.17222/mit.2021.029

The flow fields on the top and bottom surfaces of a hot-rolled strip are different during a cooling process due to the effect of gravity. This can affect the cooling uniformity of the top and bottom surfaces, and plate-curvature problems may appear. The finite-element method was used to study the plate-curvature law and a conclusion was obtained: the uniformity of the heat-transfer coefficients for the top and bottom surfaces was crucial for controlling the plate-curvature after cooling. The finite-volume method was used to calculate the heat-transfer coefficient during run-out-table laminar cooling (LC) and ultra-fast cooling (UFC) with different top-nozzle fluxes and water-flux ratios. The heat-transfer coefficient and its distribution with different cooling methods and process parameters were obtained, and some conclusions were obtained with analyses: the heat-transfer coefficients for the bottom and top surfaces can be kept nearly the same by adjusting the water-flux ratio between the bottom nozzle and top nozzle. The optimal water-flux ratios during laminar cooling were 1.20 and 1.15 when the top-nozzle fluxes were 100 m^3/h and 120 m^3/h, respectively. The optimal water-flux ratios during ultra-fast cooling were 1.08, 1.10, 1.15, 1.20 and 1.20 when the top-nozzle fluxes were (80; 100; 120; 140; 160) m^3/h, respectively. The obtained results and a water-flux-ratio calculating model were used in several strip-cooling lines of a hot-strip mill, providing a favorable effect.

Key Words: hot-rolled strip, plate-curvature, ultra-fast cooling, water-flux ratio

Zaradi gravitacije je med procesom ohlajanja tok toplotnega polja med zgornjo in spodnjo površino vrče valjanega traku različen. To lahko vpliva na enakomernost ohlajanja zgornje in spodnje površine traku. Zaradi tega se lahko prečni presek traku ukrivi. Avtorji članka so uporabili metodo končnih elementov za raziskavo procesov, ki vplivajo na ukrivljenost. Pri tem so prišli do naslednje ugotovitve: enakomernost koeficienta prenosa toplote na spodnji in zgornji površini je ključna za ohranitev geometrije pločevine pri ohlajanju. Z metodo končnih elementov so izračunavali koeficient prenosa toplote med laminarnim ohlajanjem (LC) in ultra hitrim ohlajanjem (UFC) z različnim pretokom vode skozi zgornje vodne šobe in razmerji pretoka vode. Dosegli so različne koeficiente prenosa toplote in njihovo porazdelitev glede na izbrane različne metode hlajenja. Analiza je pripomogla k nekaterim zaključkom: koeficienti prenosa toplote na zgornji in spodnji površini se lahko vzdržujejo približno na enakem nivoju z nastavitvijo primernega pretoka vode skozi zgornje in spodnje šobe. Optimalni razmerji pretoka vode za laminarno ohlajanje sta bili 1,20 in 1,15, ko sta bila zgornja pretoka vode 100 m^3/h oz. 120 m^3/h. Optimalna razmerja pretoka vode pri ultra hitrem ohlajanju so bila 1,08, 1,10, 1,15, 1,20 oziroma 1,20, ko so bili pretoki vode skozi šobe 80 m^3/h, 100 m^3/h, 120 m^3/h, 140 m^3/h oziroma 160 m^3/h. Avtorji so dosežene rezultate in modelne izračune razmerij pretoka vode uporabili na več različnih ohlajevalnih linijah vroče valjanih trakov in dosegli ugodne učinke.

Ključne besede: vroče valjan trak, ukrivljenost plošče, ultra hitro ohlajanje, razmerje pretoka vode

1 INTRODUCTION

Laminar cooling is used for most of hot-strip mills (HSMs). Currently, hot-rolled strips with high properties and low costs have been proposed, but the traditional laminar-cooling equipment has a low cooling rate and poor cooling uniformity, confine further development of the new-generation TMCP (thermo-mechanical control process)[1] while products can be obtained with ultra-fast cooling.[2,3] The controlled-rolling and controlled-cooling technologies with ultra-fast cooling are rapidly developing due to the advantages of good properties and low costs.[4,5]

Plate warping and side wave are the two common plate-curvature defects.[6,7] Plate-shape defects may also appear during ultra-fast cooling and laminar cooling performed on a run-out table because of an uneven cooling intensity so effective measures should be taken to avoid plate-curvature defects caused by uneven cooling. A hot-rolled strip is cooled by the nozzles, installed on the top and bottom of the strip, respectively. The top nozzles are installed at the top of the strip and the top-nozzle spraying direction is the same as that of the gravity. The bottom nozzles are installed at the bottom of the strip and the bottom-nozzle spraying direction is opposite to that of the gravity. Thus, the flow fields at the top and bottom of the strip are different, causing the top- and bottom-surface temperatures to be different as well.

Many scholars conducted thorough research on the plate-curvature changing law. X. D. Wang and D. Weisz-Patrault studied the residual stress and strip-flatness changing law on a run-out table and reached some

*Corresponding author's e-mail:
neu2015@163.com (Lian-yun Jiang)

valuable conclusions.[8–10] Y. L. Li and X. Y. Shan studied the profile and flatness control technology and obtained a plate-shape control strategy to keep the plate shape stable during rolling.[11,12] The plate-curvature produced during cooling on a run-out table was also studied. J. H. Shi studied the heat-transfer intensity of jet impingement in order to keep the surface temperature well-distributed.[13,14] Controlled rolling and controlled cooling technology play an important role in the development of steel materials with good properties and lower costs. Many in-depth researches were focused on the steel-material development and improvement of the strip cooling rate, especially the improvement of ultra-fast cooling intensity. B. Wang, S. Tang and Z. L. Li developed medium-carbon steels, high-strength microalloyed steels and X80 pipe steels using ultra-fast cooling after hot strip rolling.[15–17]

The flow fields on the top and bottom surfaces of a hot-rolled strip may be different because of the gravity, while the top- and bottom-nozzle fluxes are the same. So the temperatures of the top half and bottom half of the hot-rolled strip are different, and the plate-shape defect or a great residual stress may appear. Consequently, the water-flux ratio between the bottom and top-nozzle fluxes can also significantly affect the plate shape because of the gravity. Many scholars focus on the material development based on the ultra-fast cooling and the increase in the ultra-fast cooling intensity. Not many scholars conducted in-depth research from this perspective that is of key importance for industrial applications, although many in-depth researches on the plate-curvature changing law were conducted. In-depth research on the plate-curvature changing law and the method achieving the optimal plate-curvature used during run-out-table cooling were conducted in our study and a model calculated on the basis of the water-flux ratio (the flux ratio of the bottom and top nozzles) was set up to provide guidance to industry.

2 NUMERICAL MODELING

A hot-rolled strip underwent heating, rough rolling, finishing rolling, ultra-fast cooling, laminar cooling and down coiling. The arrangement of run-out-table cooling in a HSM (hot strip mill) is shown in **Figure 1**. In this figure, FM is finishing mill; FDT is finishing delivery temperature; UFCT is ultra-fast cooling temperature; CT is coiling temperature and DC is down coiler.

The finite-element method, finite-volume method and finite-difference method are common numerical algorithms. The finite-volume method can couple the temperature field and flow field very well, so it is used to calculate the heat-transfer coefficient and the finite-element method is used to calculate the thermal stress and thermal deformation.

2.1 Model of the finite-element method

The strip thickness and width are 1.0–25.0 mm and 1000–2000 mm, and the length is generally more than 100 m so the width-thickness ratio is great enough and this 3D model can be simplified as a 2D planar problem when studying the plate shape along the length or width.

The thermal stress appears during the cooling process and the thermal-structural coupling calculation is conducted according to the strip cooling process. The thermal-structural coupling element (Plane 13, in the Ansys13.0 software) and the second boundary condition (the Neumann condition, specifying the heat-transfer coefficient for every node every time) are taken during the calculation. The strip is modeled as a bilinear isotropic material. The initial temperature of the strip and the cooling-water temperature are 860 °C and 27 °C, respectively. The steel density is 7850 kg/m^3, Poisson's ratio is 0.25 and the thickness is 5.0 mm. Other parameters are listed in **Table 1**.

Strip warping and side wave are common plate-curvature problems. A strip sample with a length of 1.0 m and a thickness of 5.0 mm is taken to study the

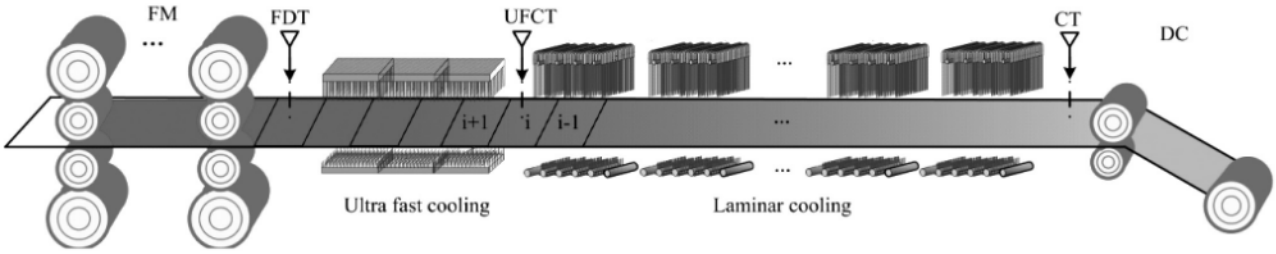

Figure 1: Arrangement of ultra-fast cooling and laminar cooling in the HSM

Table 1: Steel physical parameters at different temperatures

Temperature /°C	50	100	200	400	500	600	700	800	1000
Conductivity /W·m^{-1}·K^{-1}	51.5	50.5	48.6	42.7	39.3	35.6	31.9	25.9	27.7
Specific heat /J·kg^{-1}·°C^{-1}	448	502	519	595	662	745	846	955	645
Linear expansivity /10^{-5} °C^{-1}	1.19	1.21	1.26	1.37	1.43	1.48	1.53	1.57	1.61

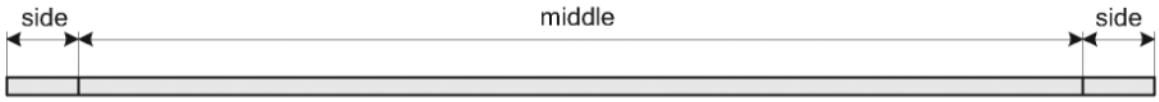

Figure 2: Side-wave distribution along the width

strip-warping deformation, affected by the heat-transfer coefficient distribution along the length of the strip. The strip cooling process can be simulated with a 2D model. Five kinds of simulations are set up in order to obtain the plate-warping changing law and the parameters are listed in **Table 2**.

Table 2: Process parameters for simulations with the same heat-transfer coefficient

No.	Item	Heat-transfer coefficient /W·(m²·K)⁻¹	
		Top surface	Bottom surface
1	Process 1	10000	10000
2	Process 2	10000	10500
3	Process 3	10000	11000
4	Process 4	10000	11500
5	Process 5	10000	12000

Side wave is another common plate-curvature problem and a strip sample with a width of 1.0 m and a thickness of 5.0 mm is taken to study the side-wave deformation, affected by the heat-transfer coefficient distribution along the width of the strip. The sample is divided into three parts, as is shown in **Figure 2**. The lengths of the side and middle parts are 0.1 m and 0.8 m, respectively. The strip cooling process is simulated with a 2D model. Five kinds of simulations are set up in order to obtain the side-wave changing law and the parameters are listed in **Table 3**, relating to the situation when the top- and bottom-surface heat-transfer coefficients are the same.

Table 3: Process parameters for simulations with different heat-transfer coefficients

No.	Item	Heat-transfer coefficient /W·(m²·K)⁻¹	
		Middle	Edge
1	Process 1'	10000	10000
2	Process 2'	10000	11000
3	Process 3'	10000	12000
4	Process 4'	10000	13000
5	Process 5'	10000	14000

2.2 Model of the finite-volume method

The ultra-fast cooling nozzle (an intensive nozzle) and laminar cooling nozzle (a U-shaped nozzle) are used for ultra-fast cooling and laminar cooling of strips, and they are made of many small round nozzles.[20] A small round nozzle can be taken out for analysis. The small nozzle is axisymmetric so it can be simplified as a 2D axial-symmetry model, as is shown in **Figure 3**.

In **Figure 3**, AB and IJ indicate the velocity inlet, m/s, VOF (volume of fraction) = 1.0, the water temperature is 27 °C; DE and HL indicate the pressure outlet, Pa, VOF (volume of fraction) = 0; AF, FG and IG indicate the symmetry axis; EFGH is the hot-rolled strip, the thickness is 10 mm, the initial temperature is 860 °C; ACDFE and IKLHG indicate the fluid region, the incompressible fluid; and the gravity is 9.8 m/s². Other parameters used in the simulation are listed in **Table 4**.

Table 4: Data used in the simulation

Material	Density /kg·m⁻³	Specific heat /J·(kg°C)⁻¹	Conductivity /W·(m·K)⁻¹	Viscosity /kg·(m·s)⁻¹	Initial temperature /°C
water	1000	998	0.6	1.003×10^{-3}	27
air	1.225	1006	0.0242	1.789×10^{-5}	27
steel	7850	448	45	–	860

When water is sprayed into the air, an energy exchange and turbulent diffusion take place; then a mixture of water and air and a residual water layer are formed in the cooling region. The spray-cooling process was simulated with the Ansys/fluent software. The mixture model can be used for the calculation in accordance with the characteristics of the three multiphase models. The strip is modeled as a solid, while the air and water are modeled as a fluid in the Ansys/fluent software. All convective terms were discretized with a second-order linear upwind scheme, and an RNG (renormalization group) k-ε model[12,13] was used for turbulence modeling. The model parameters k and ε can be calculated with Equations (1) and (3).

$$k = \left[0.16 \times (vL/\mu)^{-1/8} \times v_{\text{wall}}\right]^2 \quad (1)$$

$$L = \phi \quad (2)$$

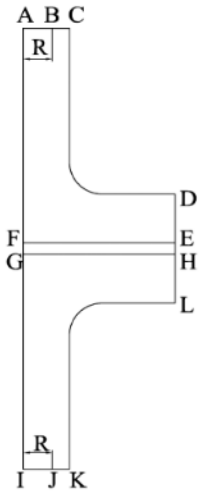

Figure 3: Round-nozzle model for a hot-rolled strip after rolling

$$\varepsilon = \frac{0.09^{3/4} k^{3/2}}{0.07L} \quad (3)$$

Here, k is the turbulent kinetic energy, m^2/s^2; ε is the turbulence dissipation rate, m^2/s^3; v is the average velocity in the section, m/s; L is the characteristic length, m; ϕ is the round-pipe diameter, m; μ is the kinematic viscosity, which is 1.002×10^{-6} m^2/s for the water at 27 °C; v_{wall} is the maximum velocity of the wall, m/s.

3 PLATE-CURVATURE AFFECTING LAW

Strip-cooling processes were simulated in accordance with the parameters listed in **Tables 1** and **2** and the node displacement at the top surface was obtained, as is shown in **Figure 4a**.

Figure 4a shows that the node displacement is nearly 0 when the top- and bottom-surface heat-transfer coefficients are equal. Strip warping appears when the top - and bottom-surface heat-transfer coefficients are different. The reason for this is the fact that the top-surface temperature is higher than the bottom-surface temperature when the bottom-surface heat-transfer coefficient is greater than the top-surface heat-transfer coefficient. The bottom surface contracts greatly compared to the top surface when the bottom-surface heat-transfer coefficient is greater than the one at the top. The warping amount is about 1.5 mm when the difference between the top- and bottom-surface heat-transfer coefficients is 500 $W\cdot(m^2\cdot K)^{-1}$, as is included in Process 2. The warping amount is about 5.5 mm when the difference between the top- and bottom-surface heat-transfer coefficients is 2000 $W\cdot(m^2\cdot K)^{-1}$, as is included in Process 5. So, the strip is warped more seriously when the difference between the top- and bottom-surface heat-transfer coefficients is greater.

Consequently, the key to avoid strip warping after cooling is to keep the top- and bottom-surface heat-transfer coefficients consistent. Certain measures should be taken to maintain the consistency of the top- and bottom-surface heat-transfer coefficients.

Strip-cooling processes were simulated in accordance with the parameters listed in **Tables 1** and **3**, and the node displacement and node temperature of the top surface were obtained, as is shown in **Figures 4b** and **5**.

Side wave is another common plate-shape problem. **Figure 4b** shows that the maximum node displacement is 0.03 mm when the difference between the heat-transfer coefficients of the side and middle parts is 4000 $W\cdot(m^2\cdot K)^{-1}$. So, a tiny side wave appears when the top- and bottom-surface heat-transfer coefficients are the same, while the heat-transfer coefficients of the side and middle parts are different. It can be concluded from the above that no apparent side wave appears after cooling if the top- and bottom-surface heat-transfer coefficients are the same, so the key to avoid a side wave after cooling is to keep the top- and bottom-surface heat-transfer coefficients consistent.

Figure 5 shows that the temperature along the width is unevenly distributed although no apparent side wave appears, as is shown in **Figure 4b**. The unevenly distributed temperature along the width is not beneficial for keeping the microstructure and property well-distributed. So, certain measures, such as edge masking or re-design-

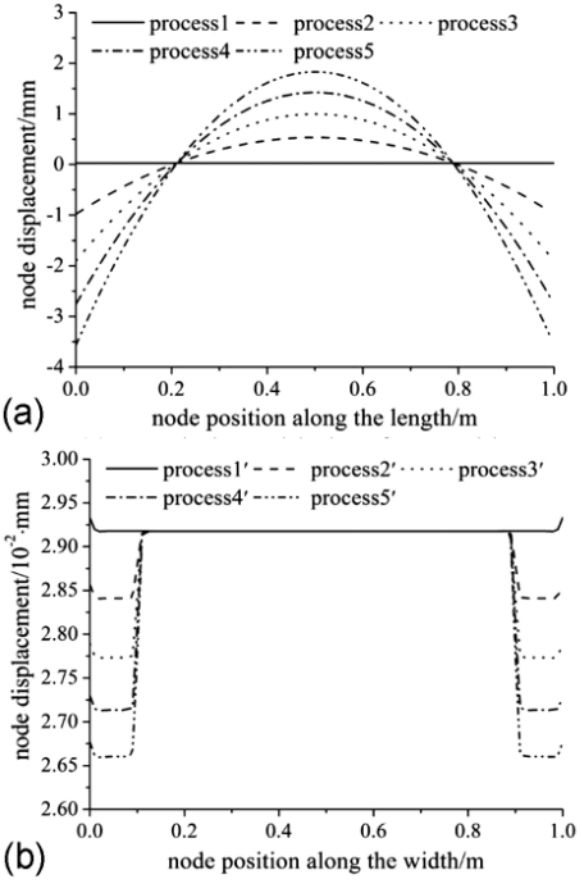

Figure 4: Node displacement on the top surface: a) caculation with data from **Table 2**, b) caculation with data from **Table 3**

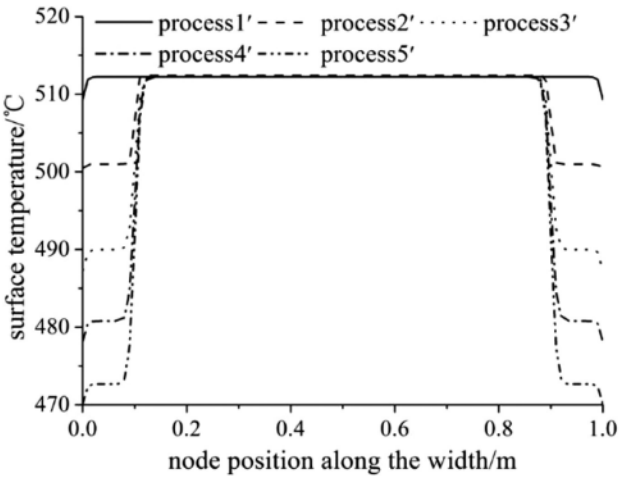

Figure 5: Node temperature on the top surface

ing the nozzle array,[17] should be taken to keep the temperature well-distributed.

4 OPTIMAL PLATE-CURVATURE ACHIEVING METHOD

The consistence of the top- and bottom-surface heat-transfer coefficients is the key measure for keeping the plate shape stable during cooling, and the top- and bottom-surface heat-transfer coefficients tend to be consistent when the water flux ratio between the bottom- and top-nozzle fluxes is adjusted. Currently, there is not any reliable model for calculating the water ratio. The finite-volume method is used to calculate the heat-transfer coefficient for different water-flux ratios in accordance with the parameters of laminar cooling and ultra-fast cooling.

4.1 Optimal water-flux ratio of laminar cooling

An overhead water tank with a height of about 7.0 m feeds the laminar-cooling nozzle. The top-nozzle diameter is about 18 mm, the outlet velocity is 1.0 m/s and the distance between the nozzle outlet and the strip is about 1.76 m. The laminar-cooling nozzle flux is generally about 100–120 m^3/h, and the laminar-cooling rate or the coiling temperature is adjusted by adjusting the amount of the nozzle flux with on-off valves. So the strip laminar-cooling processes were simulated for the situation when the top-nozzle flux is 100–120 m^3/h and the water-flux ratio is 1.0–1.20 in accordance with the initial and boundary conditions. The heat-transfer-coefficient distribution at an average surface temperature of about 500 °C was obtained, as shown in **Figure 6**. f is the water-flux ratio of the bottom-nozzle flux to top-nozzle flux. The average heat-transfer coefficients for different cooling regions were also obtained, as shown in **Table 5**, and R was the radial position.

The changing law is obtained from **Figure 6**: the heat-transfer coefficient increases gradually with the improvement in the radial position and the maximum value appears in a certain position. Then it decreases with the improvement in the radial position.

Figure 6a shows that the top-surface heat-transfer coefficient is greater than the bottom-surface heat-transfer coefficient because of the gravity that prevents the cooling water from touching the strip for a long time when the top and bottom water fluxes are the same. The cooling water cannot get in touch with the bottom surface when the radial position is greater than 0.03 m and the bottom-surface heat-transfer coefficient is 0 in this region. So it is necessary to improve the bottom-nozzle flux in order to keep the top- and bottom-surface heat-transfer coefficients nearly the same.

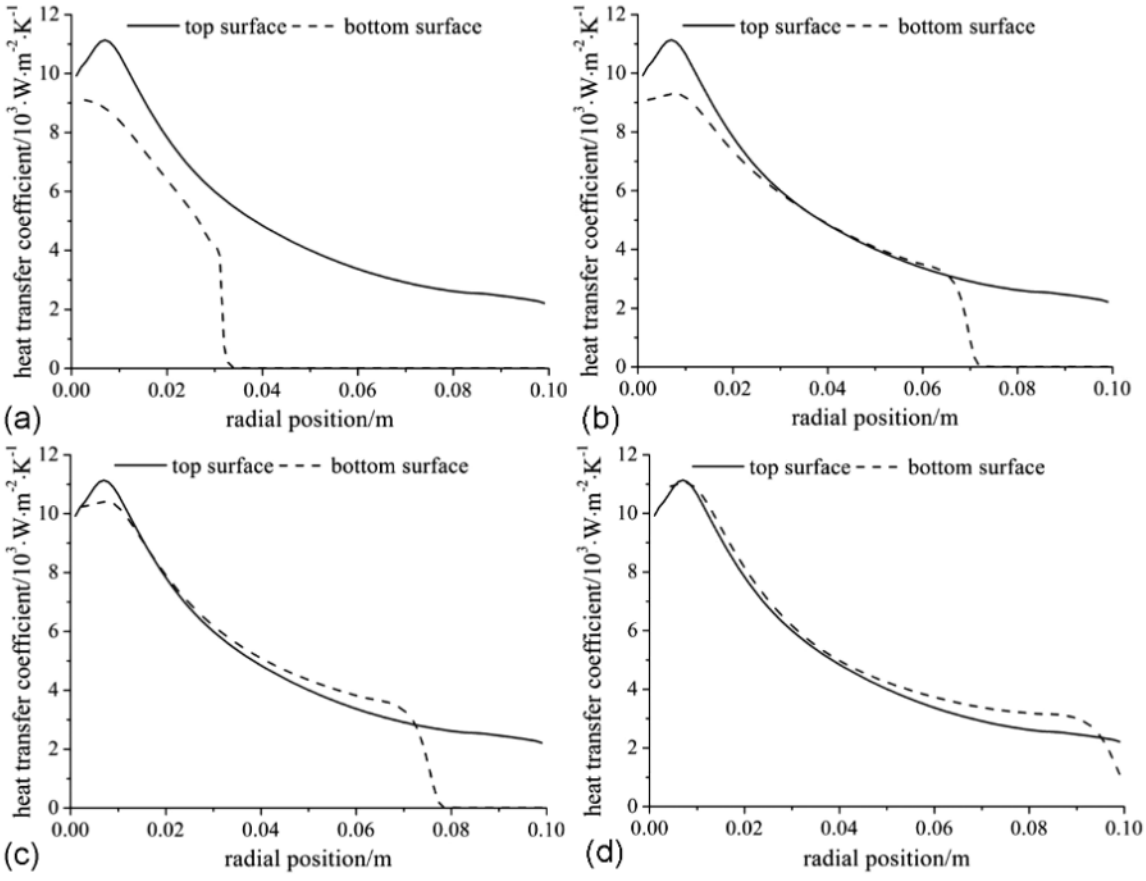

Figure 6: Heat-transfer-coefficient distribution at a water ratio of 1.0–1.20: a) f = 1.0, b) f = 1.10, c) f = 1.15, d) f = 1.20

Figure 6 shows that the contact region between the cooling water and the bottom surface expands with the improvement in the water-flux ratio. The top- and bottom-surface heat-transfer coefficients tend to be consistent with the increase in the water-flux ratio.

Table 5: Top and bottom heat-transfer coefficients within different regions

Water ratio	Average heat-transfer coefficient/W·(m²·K)⁻¹					
	Top surface			Bottom surface		
	$R \leq$ 0.01 m	$R \leq$ 0.05 m	$R \leq$ 0.1 m	$R \leq$ 0.01 m	$R \leq$ 0.05 m	$R \leq$ 0.1 m
1.0	10685	7232	5079	8884	4421	2235
1.10	10685	7232	5079	9193	6727	4056
1.15	10685	7232	5079	10301	7277	4588
1.20	10685	7232	5079	10923	7456	5368

It can be concluded from **Table 5** that the top- and bottom-surface heat-transfer coefficients tend to be consistent with the increase in the water ratio within three regions ($R \leq 0.01$ m, $R \leq 0.05$ m and $R \leq 0.1$ m). The region with $R \leq 0.1$ m is a whole cooling region and the difference between the top- and bottom-surface heat-transfer coefficients is 289 W·(m²·K)⁻¹; it is the least when the water ratio is 1.20. So the optimal water ratio is 1.20 when the top-nozzle flux is 100 m³/h during laminar cooling.

Strip-cooling processes were simulated when the top-nozzle flux was 120 m³/h and the water-flux ratio was 1.0–1.20 in accordance with the initial and boundary conditions. The average heat-transfer coefficients in different cooling regions were obtained, as shown in **Table 6**. The heat-transfer coefficient distribution at an average surface temperature of about 500 °C was also obtained, as shown in **Figure 7**.

Table 6: Top and bottom heat-transfer coefficients within different regions

Water ratio	Average heat-transfer coefficient/W·(m²·K)⁻¹					
	Top surface			Bottom surface		
	$R \leq$ 0.01 m	$R \leq$ 0.05 m	$R \leq$ 0.1 m	$R \leq$ 0.01 m	$R \leq$ 0.05 m	$R \leq$ 0.1 m
1.0	17328	9743	6440	11642	7855	5592
1.10	17328	9743	6440	13742	9037	6295
1.15	17328	9743	6440	15087	9698	6745
1.20	17328	9743	6440	15841	10203	7038

Figure 7a shows that the top- and bottom-surface heat-transfer coefficients are nearly the same when the radial position is greater than 0.03 m, but the difference is great when the radial position is less than 0.03 m. The

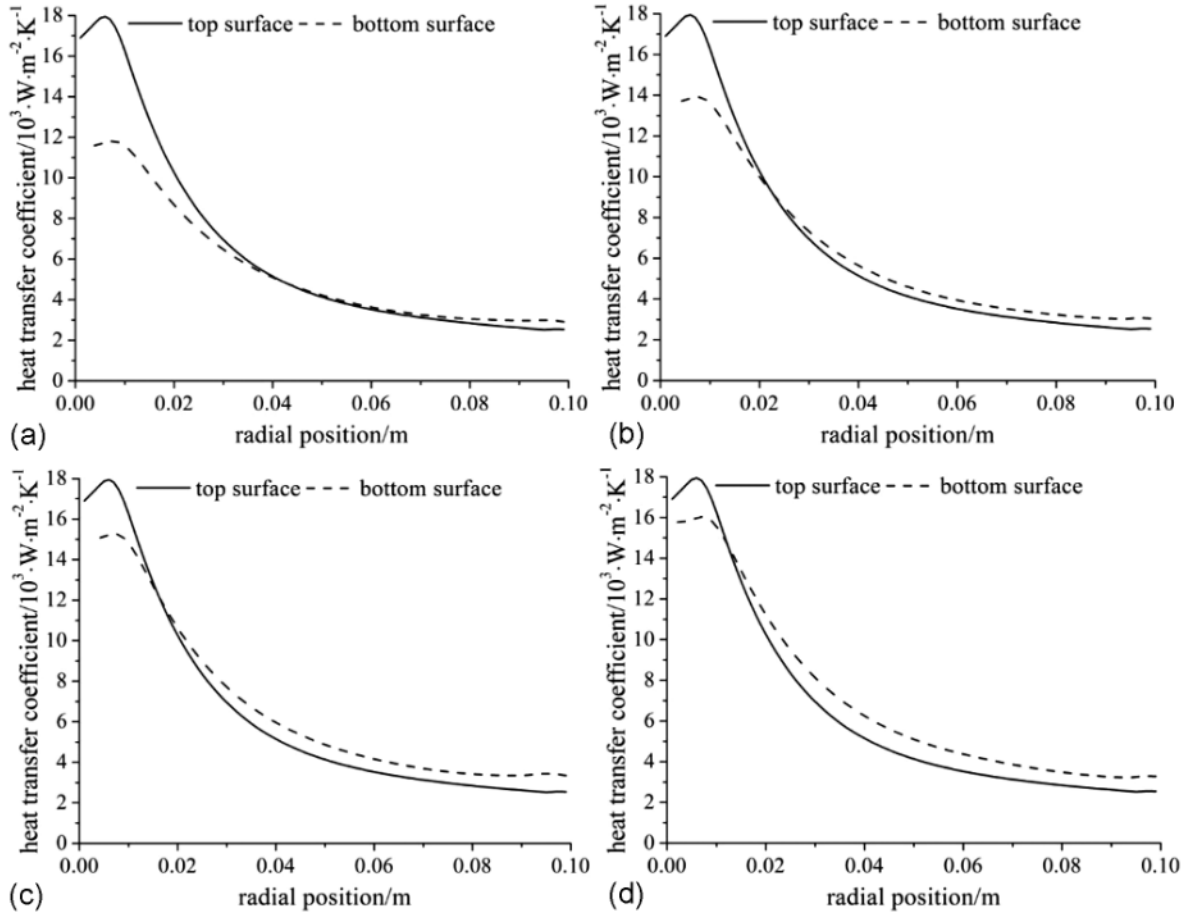

Figure 7: Heat-transfer coefficient distribution when the water ratio is 1.0–1.20: a) $f = 1.0$, b) $f = 1.10$, c) $f = 1.15$, d) $f = 1.20$

difference between the top- and bottom-surface heat-transfer coefficients at the radial position $R \leq 0.03$ decreases with the increase in the water-flux ratio.

It can be understood from **Figure 7** and **Table 6** that the top- and bottom-surface heat-transfer coefficients tend to be consistent when the water-flux ratio increases from 1.0 up to 1.15. The bottom-surface heat-transfer coefficient is much higher than the top-surface heat-transfer coefficient, which is not beneficial for controlling the plate-curvature; so the optimal water-flux ratio is 1.15 when the top-nozzle flux is 120 m^3/h during laminar cooling.

4.2 Optimal water-flux ratio of ultra-fast cooling

The ultra-fast-cooling nozzle flux is generally about 80–160 m^3/h, and the ultra-fast-cooling rate, or the coiling temperature, is also adjusted by adjusting the amount of the nozzle flux with on-off valves. The ultra-fast-cooling processes were simulated with different water-flux ratios when the top nozzle flux is 80–160 m^3/h. Processes of ultra-fast cooling of strips were simulated for the situation when the top-nozzle flux is 80 m^3/h and the water-flux ratio is 1.0–1.20 in accordance with the initial and boundary conditions. The average heat-transfer coefficients in different cooling regions were obtained, as shown in **Table 7**. The heat-transfer coefficient distribution at the average surface temperature of about 500 °C was also obtained, as shown in **Figure 8**.

Table 7: Average heat-transfer coefficients for different regions at a top-nozzle flux of 80 m^3/h

Water ratio	Average heat transfer coefficient/W/(m^2·K)					
	Top surface			Bottom surface		
	$R \leq$ 0.01 m	$R \leq$ 0.03 m	$R \leq$ 0.05 m	$R \leq$ 0.01 m	$R \leq$ 0.03 m	$R \leq$ 0.05 m
1.0	13152	8421	6131	12359	7152	4868
1.05	13152	8421	6131	12964	8017	5755
1.08	13152	8421	6131	13603	8430	6032
1.10	13152	8421	6131	14108	8750	6255

Figure 8 shows the heat-transfer coefficient distribution at different water-flux ratios and a top-nozzle flux of 80 m^3/h; it also shows that the surface heat-transfer coefficient decreases with the improvement in the radial position. The bottom-surface heat-transfer coefficient undergoes changes with different water-flux ratios. The top- and bottom-surface heat-transfer coefficients tend to be consistent with the increase in the water-flux ratio. So adjusting the water-flux ratio is an effective way of keeping the top- and bottom-surface heat-transfer coefficients consistent.

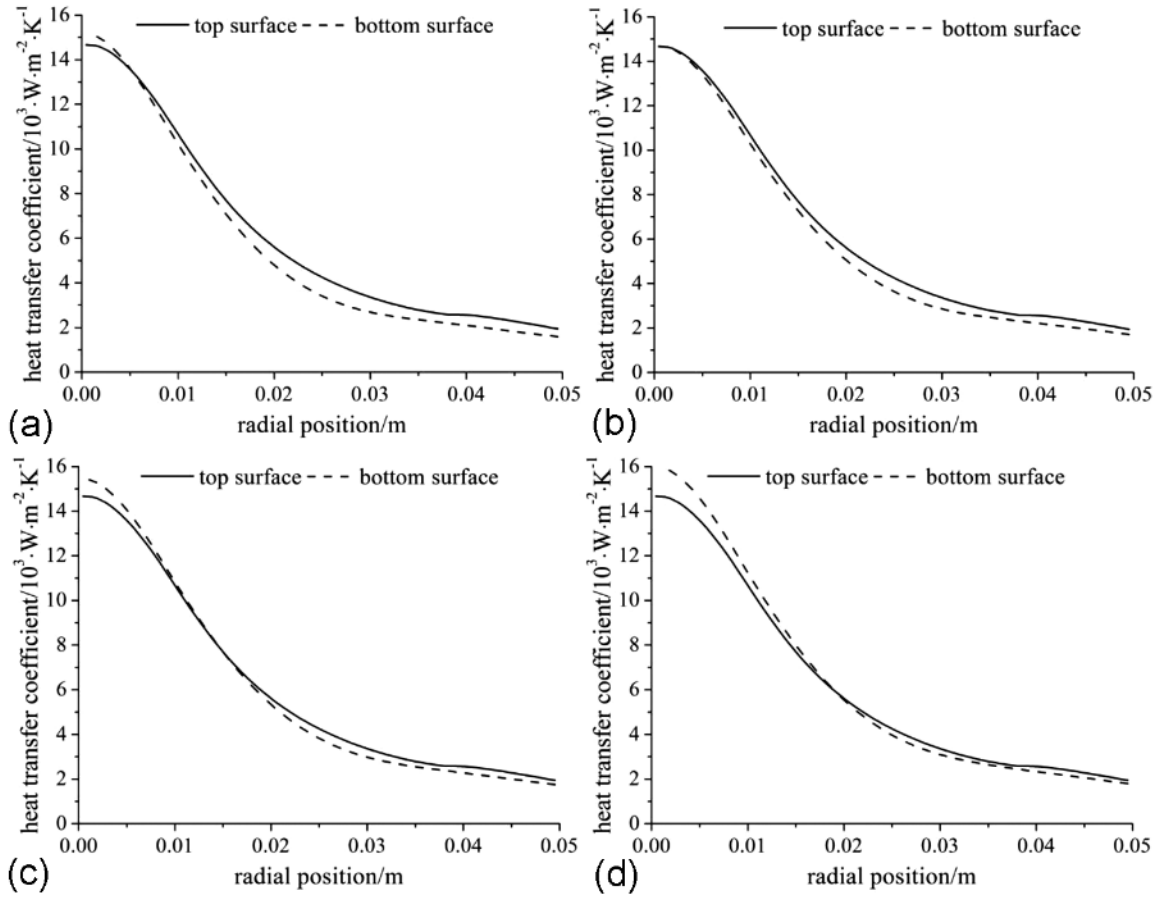

Figure 8: Heat-transfer coefficient distribution at the top-nozzle flux of 80 m^3/h and water ratio of 1.0-1.10: a) f = 1.0, b) f = 1.05, c) f = 1.08, d) f = 1.10

Figure 8 and **Table 7** show that the difference between the top- and bottom-surface heat-transfer coefficients is 188 W·(m^2·K)$^{-1}$ and it is the least within the region $R \leq 0.01$ m when the water-flux ratio is 1.05. The difference is 9 W·(m^2·K)$^{-1}$ and it is the least within the region $R \leq 0.03$ m when the water-flux ratio is 1.08. The difference is 99 W·(m^2·K)$^{-1}$ and it is the least within the region $R \leq 0.05$ m when the water-flux ratio is 1.08. The region $R \leq 0.05$ m is a whole cooling region, so the optimal water-flux ratio is 1.08 when the top-nozzle flux is 80 m^3/h during ultra-fast cooling in accordance with the heat-transfer coefficient distribution and the values of the average heat-transfer coefficients in the three cooling regions.

Processes of ultra-fast cooling of strips were simulated for the situation when the top-nozzle flux was 120 m^3/h and water-flux ratio was 1.0–1.20 in accordance with the initial and boundary conditions. The heat-transfer coefficient distribution at the average surface temperature of about 500 °C was obtained, as shown in **Figure 9**. The average heat-transfer coefficients for different cooling regions were also obtained, as shown in **Table 8**.

Figure 9a shows that the top-surface heat-transfer coefficient is greater than the bottom-surface heat-transfer coefficient in the whole cooling region ($R \leq 0.05$ m) and the difference decreases with the increase in the water ratio, as is shown in **Figure 9**. So this is an effective way of keeping the top- and bottom-surface heat-transfer coefficients consistent. It is hard to obtain the optimal water ratio from **Figure 9** because the difference in the heat-transfer coefficient is so little. And the average heat-transfer coefficient is used to obtain the optimal water ratio, as is shown in **Table 8**.

Table 8: Average heat-transfer coefficients for different regions at the top flux of 120 m^3/h

Water ratio	Average heat-transfer coefficient/W/(m^2·K)					
	Top surface			Bottom surface		
	$R \leq$ 0.01 m	$R \leq$ 0.03 m	$R \leq$ 0.05 m	$R \leq$ 0.01 m	$R \leq$ 0.03 m	$R \leq$ 0.05 m
1.0	19818	12550	9210	16437	10725	7760
1.10	19818	12550	9210	19294	12455	8994
1.15	19818	12550	9210	19277	12558	9182
1.20	19818	12550	9210	19148	12697	9232

Table 8 shows that the bottom-surface heat-transfer coefficient improves greatly when the water-flux ratio improves from 1.0 up to 1.10, but it does not change so

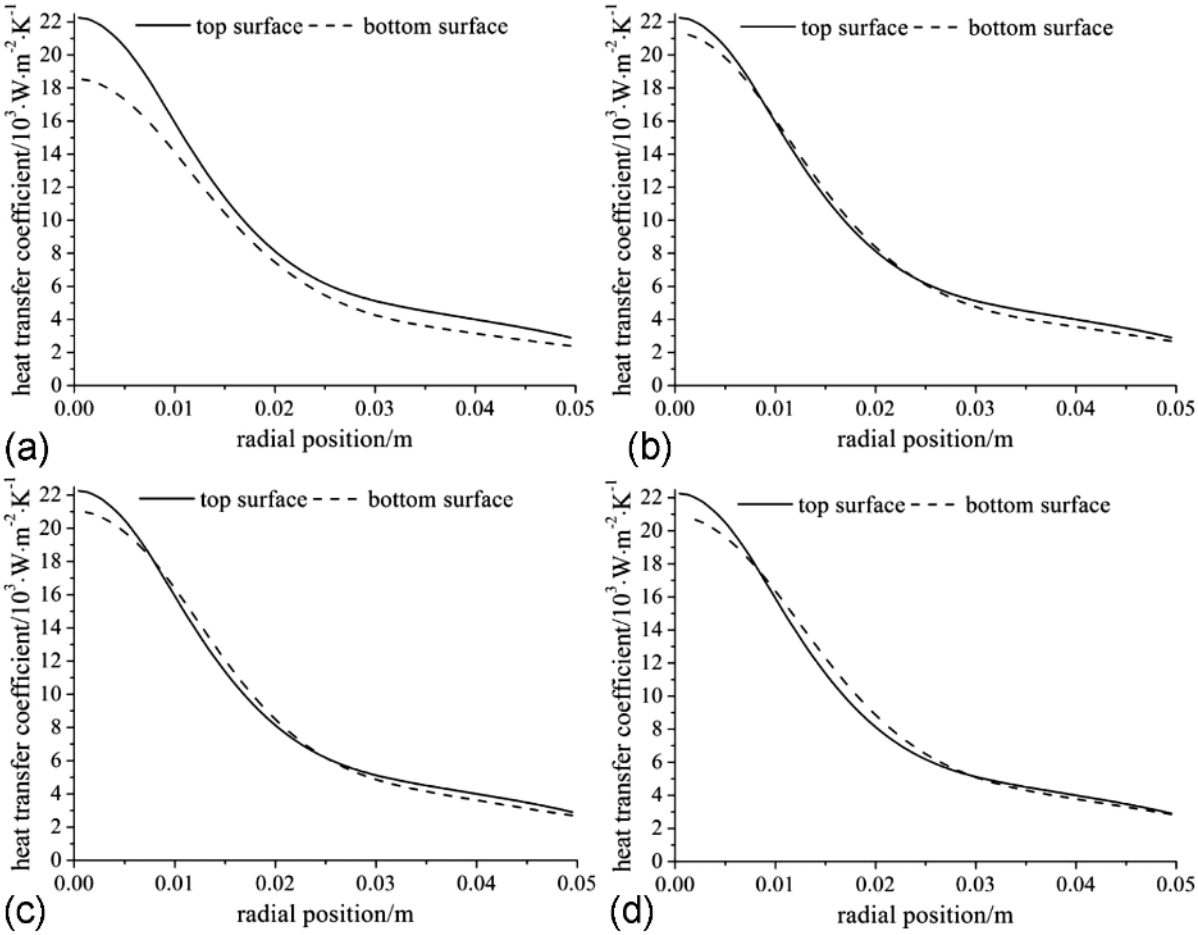

Figure 9: Heat-transfer coefficient distribution at a top-nozzle flux of 120 m^3/h and water ratio of 1.0–1.20: a) f = 1.0, b) f = 1.10, c) f = 1.15, d) f = 1.20

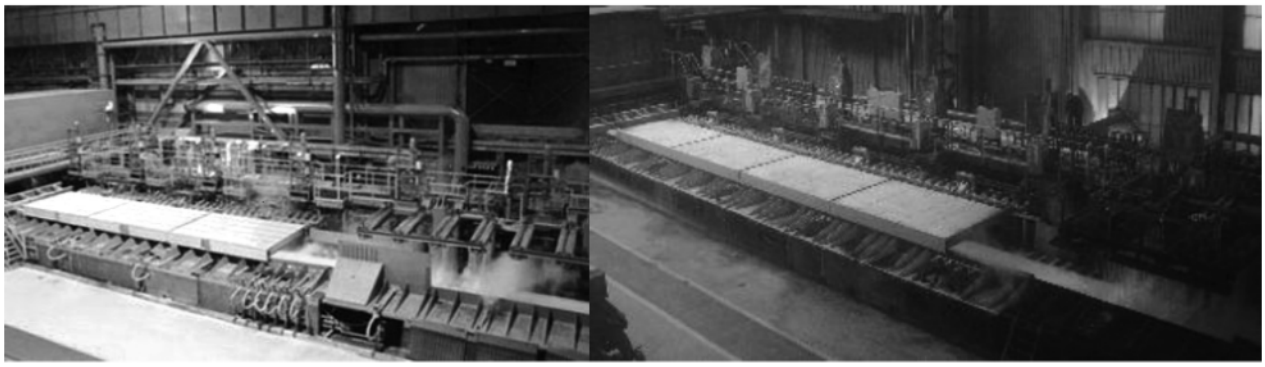

Figure 10: Ultra-fast cooling equipment of the HSMs: a) Qian'an Iron & Steel, China, b) JingTang United Iron & Steel, China

greatly when the water ratio is up to 1.10. The reason for this is the fact that the water layer at the bottom becomes thick, reducing the cooling-water contact with the hot surface. The average bottom-surface heat-transfer coefficients are 9182 $W\cdot(m^2\cdot K)^{-1}$ and 9232 $W\cdot(m^2\cdot K)^{-1}$ when the water-flux ratios are 1.15 and 1.20, respectively, at the radial position $R \leq 0.05$ m. The average top-surface heat-transfer coefficients in this region are nearly the same. The differences between the average top- and bottom-surface heat-transfer coefficients at the radial positions $R \leq 0.01$ m and $R \leq 0.03$ m are 541 $W\cdot(m^2\cdot K)^{-1}$ and 8 $W\cdot(m^2\cdot K)^{-1}$, respectively, when the water ratio is 1.15. The differences between the average top- and bottom-surface heat-transfer coefficients at the radial positions $R \leq 0.01$ m and $R \leq 0.03$ m are 670 $W\cdot(m^2\cdot K)^{-1}$ and 147 $W\cdot(m^2\cdot K)^{-1}$, respectively, when the water ratio is 1.20. So the optimal water ratio is 1.15 when the top-nozzle flux is 120 m^3/h during ultra-fast cooling, which can be seen from the difference between the top- and bottom-surface heat-transfer coefficients.

The optimal water ratio can also be obtained when the top-nozzle fluxes are (100; 140; 160) m^3/h in accordance with the top- and bottom-surface heat-transfer coefficient distribution and average heat-transfer coefficient with different water ratios. The optimal water ratios are 1.10, 1.20 and 1.20, respectively, when the top-nozzle fluxes are (100; 140; 160) m^3/h. The optimal water ratios at different top-nozzle fluxes during laminar cooling and ultra-fast cooling are listed in **Table 9**.

Table 9: Optimal water-flux ratio with different cooling processes

Cooling method	Top-nozzle flux /$m^3\cdot h^{-1}$	Optimal water ratio
Laminar cooling	100	1.20
	120	1.15
Ultra-fast cooling	80	1.08
	100	1.10
	120	1.15
	140	1.20
	160	1.20

Table 9 shows that the optimal water ratio increases with the increase in the top-nozzle flux during ultra-fast cooling, and it remains constant when the top-nozzle flux is up to 140 m^3/h.

An equation that is used for calculating the optimal water ratio during ultra-fast cooling is obtained with the least-square method[18,19] in accordance with the calculated data:

$$f = a_1\left(\frac{Q}{Q_0}\right)^3 + a_2\left(\frac{Q}{Q_0}\right)^2 + a_3\left(\frac{Q}{Q_0}\right) + a_4 \qquad (4)$$

where f is the water-flux ratio during ultra-fast cooling; Q is the total top-nozzle flux, m^3/h; Q_0 is the basic nozzle flux, 100 m^3/h; a_1, a_2, a_3, a_4 are model parameters, $a_1 = -0.625$, $a_2 = 2.25$, $a_3 = -2.43$, $a_4 = 1.9$.

5 PRACTICAL EXPERIMENT AND APPLICATIONS

The obtained optimal-water-ratio calculating model for laminar cooling and ultra-fast cooling was used in 2160 mm HSM of Qian'an Iron and Steel in China, 2250 mm HSM of Shougang Jingtang United Iron and Steel in China and CSP Line of Baotou Iron and Steel in China, where favourable results were obtained. **Figure 10** shows the strip cooling during ultra-fast cooling and laminar cooling in Qian'an Iron and Steel and Shougang Jingtang United Iron and Steel, respectively.

Figure 10 shows that the strip is flat after ultra-fast cooling and laminar cooling and the plate shape is less than 30*I*, as measured with a flatness meter, proving that the water-flux-ratio calculating model is reliable.

6 CONCLUSIONS

(1) The difference between the top- and bottom-surface heat-transfer coefficients can affect the plate shape during run-out-table cooling. The plate shape is stable if the top- and bottom-surface heat-transfer coefficients are the same. No apparent plate-shape defect occurs; however, the temperature is not well distributed along the width if the top- and bottom-surface heat-transfer coefficients are the same while the heat-transfer coefficients in the edge and middle parts are different. So the consistency of the top- and bottom-surface heat-transfer coeffi-

cients is of key importance for keeping the plate shape stable during cooling on a run-out table.

(2) The flow fields on the top and bottom surfaces are different when the top- and bottom-nozzle fluxes are the same because of gravity. The top- and bottom-surface heat-transfer coefficients and their distribution tend to be consistent if we adjust the water-flux ratio between the bottom- and top-nozzle fluxes. So adjusting the water-flux ratio is an effective way of keeping the plate shape stable.

(3) The heat-transfer coefficient during laminar cooling was calculated with the finite-volume method and the optimal water-flux ratio was obtained with an analysis. The optimal water-flux ratios were 1.20 and 1.15 when the top-nozzle fluxes were 100 m^3/h and 120 m^3/h, respectively, during laminar cooling.

(4) The heat-transfer coefficient during ultra-fast cooling was calculated with the finite-volume method and the optimal water-flux ratio was obtained with an analysis. The optimal water-flux ratios were 1.08, 1.10, 1.15, 1.20 and 1.20 when the top-nozzle fluxes were (80; 100; 120; 140; 160) m^3/h, respectively, and the water-ratio calculating model was obtained with the least-square method.

Acknowledgments

This research was financially supported by the National Natural Science Foundation of China (Grant no. 51804206) and Open Research Fund from the State Key Laboratory of Rolling and Automation, Northeastern University (2020RALKFKT010).

7 REFERENCES

[1] E. El-Shenawy, R. Reda, Optimization of TMCP strategy for microstructure refinement and flow-productivity characteristics enhancement of low carbon steel, J. Mater. Res. Technol., 8 (**2019**) 3, 2819–2831, doi:10.1016/j.jmrt.2019.04.021

[2] J. Zhao, W. Hu, X. Wang, J. Kang, G. Yuan, H. Di, R. D. K. Misra, Effect of microstructure on the crack propagation behavior of microalloyed 560MPa (X80) strip during ultra-fast cooling, Mat. Sci. Eng. A-Struct., 666 (**2016**) 1, 214–224, doi:10.1016/j.msea.2016.04.073

[3] X. G. Zhou, Z. Y. Liu, S. Y. Song, D. Wu, G. D. Wang, Upgrade rolling based on ultra-fast cooling technology for C-Mn steel, J. Iron Steel Res. Int., 21 (**2014**) 1, 86–90, doi:10.1016/S1006-706X(14)60013-3

[4] X. L. Li, C. S. Lei, X. T. Deng, Z. D. Wang, Y. G. Yu, G. D. Wang, R. D. K. Misra, Precipitation strengthening in titanium microalloyed high-strength steel plates with new generation-thermomechanical controlled processing (NG-TMCP), J. Alloy Compd., 689 (**2016**) 12, 542–553, doi:10.1016/j.jallcom.2016.08.010

[5] W. Tan, B. Han, S. Z. Wang, Y. Yang, C. Zhang, Y. K. Zhang, Effects of TMCP parameters on microstructure and mechanical properties of hot rolled economical dual phase steel in CSP, J. Iron Steel Res. Int., 19 (**2012**) 6, 37–41, doi:10.1016/S1006-706X(12)60124-1

[6] S. Abdelkhalek, P. Montmitonnet, N. Legrand, P. Buseeler, Coupled approach for flatness prediction in cold rolling of thin strip, Int. J. Mech. Sci., 53 (**2011**) 9, 661–675, doi:10.1016/j.ijmecsci.2011.04.001

[7] D. C. Tran, N. Tardif, A. Limam, Experimental and numerical modeling of flatness defects in strip cold rolling, Int. J. Solids Struct., 69 (**2015**) 9, 343–349, doi:10.1016/j.ijsolstr.2015.05.017

[8] X. D. Wang, F. Li, Q. Yang, A. R. He, FEM analysis for residual stress prediction in hot rolled steel strip during the run-out table cooling, Appl. Math. Model., 37 (**2013**) 1–2, 586–609, doi:10.1016/j.apm.2012.02.042

[9] D. Weisz-Patrault, T. Koedinger, Residual stress on the run out table accounting for multiphase transitions and transformation induced plasticity, Appl. Math. Model., 60 (**2018**) 4, 18–33, doi:10.1016/j.apm.2018.02.026

[10] X. D. Wang, F. Li, Z. Y. Jiang, Thermal, microstructural and mechanical coupling analysis model for flatness change prediction during run-out table cooling in hot strip rolling, J. Iron Steel Res. Int., 19 (**2012**) 9, 43–51, doi:10.1016/S1006-706X(13)60007-2

[11] Y. L. Li, J. G. Cao, N. Kong, D. Wen, H. H. Ma, Y. S. Zhou, Profile and flatness control technology with a long shifting stroke on wide non-oriented electrical steel sheets, Steel Res. Int., 88 (**2017**) 4, 1–7, doi:10.1002/srin.201600208

[12] X. Y. Shan, H. M. Liu, C. Y. Jia, J. L. Sun, Flatness and profile integration control model for tandem cold mills, J. Iron Steel Res. Int., 19 (**2012**) 3, 31–37, doi:10.1016/S1006-706X(12)60070-3

[13] J. H. Shi, G. Yuan, L. Y. Jiang, Z. L. Li, K. Zhao, G. D. Wang, Heat transfer symmetry of the strip surface due to a group oblique slot jet impingement after hot rolling, Steel Res. Int., 86 (**2015**) 12, 1548–1557, doi:10.1002/srin.201400529

[14] J. H. Shi, G. Yuan, L. Y. Jiang, K. Zhao, G. D. Wang, Numerical analysis of heat transfer intensity from twin slot vertical jet impingement on strip surface after hot rolling, J. Cent. South Univ., 22 (**2015**) 7, 2816–2824, doi:10.1007/s11771-015-2813-2

[15] B. Wang, Z. Y. Liu, X. G. Zhou, G. D. Wang, Improvement of hole-expansion property for medium carbon steels by ultra-fast cooling after hot strip rolling, J. Iron Steel Res. Int., 20 (**2013**) 6, 25–32, doi:10.1016/S1006-706X(13)60107-7

[16] S. Tang, Z. Y. Liu, G. D. Wang, R. D. K. Misra, Microstructural evolution and mechanical properties of high strength microalloyed steels: Ultra-Fast Cooling (UFC) versus Accelerated Cooling (ACC), Mat. Sci. Eng. A-Struct., 580 (**2013**) 9, 257–265, doi:10.1016/j.msea.2013.05.016

[17] Z. L. Li, D. Chen, Y. J. Li, X. Q. Wang, J. Kang, G. Yuan, A novel process involving multiple strengthening mechanisms for production of low-residual stress X80 pipe steel based on ultra-fast cooling, Materials Letters, 257 (**2019**) 10, 1–4, doi:10.1016/j.matlet.2019.126767

[18] Z. T. Huang, D. Lei, Z. Han, J. Lin, Boundary moving least squares method for 3D elasticity problems, Eng. Anal. Bound. Ele., 121 (**2020**) 10, 255–266, doi:10.1016/j.enganabound.2020.10.010

[19] T. Q. Gu, Y. Tu, D. W. Tang, S. W. Lin, B. Fang, A trimmed moving total least-squares method for curve and surface fitting, Meas. Sci. Technol., 31 (**2020**) 4, 1–8, doi:10.1088/1361-6501/ab4ff6

[20] L. Y. Jiang, C. J. Zhao, J. H. Shi, D. Wu, F. D. Wang, Nozzle spray diffusivity changing law for ultra-fast cooling in hot strip mill, Journal of Donghua University (Eng. Ed.), 32 (**2015**) 4, 64–69